Gassenmeier, M., Sens-Schönfelder, C., Delatre, M., Korn, M. (2015): Monitoring of environmental influences on seismic velocity at the geological storage site for CO2 in Ketzin (Germany) with ambient seismic noise. - *Geophysical Journal International*, *200*, 1, p. 524-533

DOI: http://doi.org/10.1093/gji/ggu413

Geophysical Journal International

Geophys. J. Int. (2015) **200,** 524–533 doi: 10.1093/gji/ggu413
GJI Seismology

Monitoring of environmental influences on seismic velocity at the geological storage site for CO_2 in Ketzin (Germany) with ambient seismic noise

M. Gassenmeier,[1,2] C. Sens-Schönfelder,[1] M. Delatre[3] and M. Korn[2]

[1] *Helmholtz Centre Potsdam, German Research Centre for Geosciences GFZ, Telegrafenberg, Section* 2.4, *D*-14473 *Potsdam, Germany. E-mail: martina.gassenmeier@gfz-potsdam.de*
[2] *Institute of Geophysics and Geology, University Leipzig, Talstraße* 35, *D*-04103 *Leipzig, Germany*
[3] *BRGM,* 3 *av. Claude Guillemin, F*-45060 *Orléans Cédex* 2, *France*

Accepted 2014 October 20. Received 2014 October 17; in original form 2014 February 11

SUMMARY

Regarding the exploitation of natural resources, storage of waste or subsurface construction, there is an increasing need to obtain comprehensive knowledge about the subsurface and its temporal changes. We investigate the possibility of a passive monitoring using ambient seismic noise, which is cheap and continuous compared to active seismics. We work with data acquired with a seismic network in Ketzin (Germany) where 67 271 tons of CO_2 were injected from 2008 June until 2013 August into a saline aquifer at a depth of about 650 m. Monitoring the expansion of the CO_2 plume is essential for the characterization of the reservoir as well as the detection of potential leakage. By cross-correlating about 4 yr of passive seismic data in a frequency range of 0.05–4.5 Hz we found periodic velocity variations with a period of approximately 1 yr that cannot be caused by the CO_2 injection. The prominent direction of the noise wavefield indicates a wind farm as the dominant source providing the temporally stable noise field. This spacial stability excludes variations of the noise source distribution as a cause of spurious velocity variations. Based on an amplitude decrease associated with time windows towards later parts of the coda, we show that the variations must be generated in the shallow subsurface. A comparison to groundwater level data reveals a direct correlation between depth of the groundwater level and the seismic velocity. The influence of ground frost on the seismic velocities is documented by a sharp increase of velocity when the maximum daily temperature stays below 0 °C. Although the observed periodic changes and the changes due to ground frost affect only the shallow subsurface, they mask potential signals of material changes from the reservoir depths.

Key words: Interferometry; Hydrogeophysics; Hydrology; Wave scattering and diffraction.

1 INTRODUCTION

One of the most common methods for long term monitoring of reservoirs, CO_2 storage sites or geothermal energy production is active seismics. Passive methods based on ambient seismic noise received much attention in recent years and might present a more cost effective approach to accomplish the important task of long term monitoring. Riahi *et al.* (2013) directly analysed surface wave noise above an underground gas storage facility. Between two campaigns in April and November they could identify a change in the magnitude of anisotropy parameters for lower frequencies, which could be related to pore pressure changes in the reservoir. Our goal is to investigate the potential of noise correlation based Passive Image Interferometry (PII; Sens-Schönfelder & Wegler 2011) for reservoir monitoring at the pilot site for CO_2 storage in Ketzin (Germany).

The principle of PII is to use ambient seismic noise to calculate noise crosscorrelation functions (NCFs) that represent approximations of the Green's function between seismic stations at different times. By comparing these NCFs one can observe perturbations in the propagation of elastic waves in the subsurface, which can be caused by changes in wave velocity or attenuation. The first part of retrieving Green's function approximations is often referred to as Seismic Interferometry (SI) that states that the correlation of a random wavefield recorded by distant receivers converges towards the complete Green's function of the medium between the receivers (plus its time reversed counter-part) for a sufficient coverage of the wave vector space (Snieder 2004; Wapenaar 2004; Weaver & Lobkis

2004). If the distribution of propagation directions is not isotropic the NCFs are asymmetric and represent a poorer approximation of the Green's function. Practically the coda of earthquake records and ambient seismic noise can be used as source wavefield for SI (Campillo 2006; Larose *et al.* 2006) as was first demonstrated by Campillo & Paul (2003) and Shapiro *et al.* (2005). By extracting surface waves (Brenguier *et al.* 2007; Lin *et al.* 2009; Stehly *et al.* 2009) or body waves (Roux 2005; Tonegawa *et al.* 2009; Zhan *et al.* 2010; Poli *et al.* 2012; Lin *et al.* 2013; Nishida 2013) local, regional and global tomographic investigations of the subsurface velocity are among the most widely used applications of SI.

Not only the subsurface velocity is of high interest, with SI it is also possible to measure velocity changes as NCFs can be computed repeatedly. The comparison of such NCFs from different times is the second step of PII that usually makes use of the high sensitivity of scattered coda waves to changes of subsurface properties (Poupinet *et al.* 1984; Snieder *et al.* 2002). This allows to monitor tiny velocity changes very precisely down to a fraction of 1 per cent, for example 0.2 per cent reported by Poupinet *et al.* (1984), 0.1 per cent by Sens-Schönfelder & Wegler (2006) or 0.05 per cent by Brenguier *et al.* (2008b).

Temporal changes have been successfully detected directly after large earthquakes as a sudden drop in seismic velocity and a slow recovery afterwards (Brenguier *et al.* 2008a; Wegler *et al.* 2009; Richter *et al.* 2014). Monitoring of active volcanoes showed a drop in seismic velocity before eruptions (Brenguier *et al.* 2008b; Sens-Schönfelder *et al.* 2014). Mainsant *et al.* (2012) used noise correlation monitoring to detect material changes prior to landslides and Sens-Schönfelder & Larose (2010) applied the method to lunar data, observing changes related to thermal stress. Seasonal changes of seismic velocity have been reported by various authors: Hillers *et al.* (2014), Hobiger *et al.* (2012), Meier *et al.* (2010) and Sens-Schönfelder & Wegler (2006). The latter present a depth dependent hydrological model, describing these changes as a result of precipitation. As variations in the groundwater table are very shallow, Meier *et al.* (2010) raised the question whether variations due to temperature induced thermoelastic strain could play a more important role than precipitation. Induced thermoelastic strain persists down to a depth comparable to the lateral wavelength of the surface temperature field (Ben-Zion & Leary 1986). However, Tsai (2011) compared observed seasonal changes in California with modelled changes from poroelastic and direct elastic effects of a modelled varying groundwater table and changes modelled from thermoelastic strain variations and he concludes that the direct elastic effects of a varying groundwater table appear to have the strongest influence. Richter *et al.* (2014) observed daily velocity variations at a station in Chile in the Atacama desert with arid conditions. These velocity variations directly correlate with temperature variations. The same station shows annual velocity variations which can be modelled by thermally induced stress.

The question of how to obtain precise information about the depth where the change occurs, is a topic of ongoing research. Obermann *et al.* (2013) showed that the depth sensitivity in the early time windows of the coda is dominated by surface waves and in later time windows dominated by bulk waves, which leads to the possibility to discriminate between changes close to the surface and changes at depth.

Xu *et al.* (2012) cross-correlated noise between two profiles, that were designed for an active survey at the test-site for CO_2 storage in Ketzin, Germany. The obtained surface and reflected wave velocities do not show any discrepancies compared to the values obtained with active seismics, demonstrating that the prerequisites for the applicability of seismic interferometry in this area are met. In the following, we will introduce the site of our investigations in Section 2 and describe the characteristics of the noise field in Section 3. In Section 4, we describe the application of PII that leads to the observation of seismic velocity changes. A discussion of the observed changes and their significance at the investigation site is found in Section 5 before we finish with conclusions in Section 6.

2 THE CO_2-STORAGE SITE KETZIN

The target of this investigation is the onshore test site for CO_2 storage in Ketzin (Brandenburg, Germany). The subsurface structure of the storage site is well known from a 3-D surface seismic survey (Juhlin *et al.* 2007) performed prior to injection and from well logs (Förster *et al.* 2006) as well as from surface wave analysis of the shallow subsurface (Xu *et al.* 2012). Between 2008 June and 2013 August supercritical CO_2 was injected at a depth of about 650 m into a saline aquifer, the Stuttgart formation with a thickness of approximately 80 m (Fig. 1a). The Stuttgart Formation is lithologically heterogeneous and consists of high-permeability sandy channel-(string)-facies rocks alternating with muddy flood-plain-facies rocks of poor reservoir quality. A 210-m-thick caprock of playa-type mudstones of the Weser and Arnstadt formations is located above the injection horizon (Förster *et al.* 2006). Until the end of injection in 2013 August, in total 67 271 tons of CO_2 were stored in the formation. This is a relatively small amount compared to other injection sites like the Sleipner field, where 1.9 Mt were injected between 1999 and 2001 (Arts *et al.* 2004) or the In Salah project (2.5 Mt between 2004 and 2008, Ringrose *et al.* 2009). Time-lapse monitoring in 3-D between 2005 and 2011 (Ivanova *et al.* 2012) with active reflection seismics indicates an asymmetric CO_2 plume with an extension of 250 m in N–S direction and about 350 m in the E–W direction containing a larger amount of CO_2 in the western part.

We operated a seismic network around the test-site from 2008 May (before the beginning of the injection) until 2010 June, mainly equipped with 3c-Guralp seismometers, with eigenperiods of 60 s operating with a sampling rate of 100 Hz. During 2011 February, the network was re-equipped and extended from 5 to 10 receivers

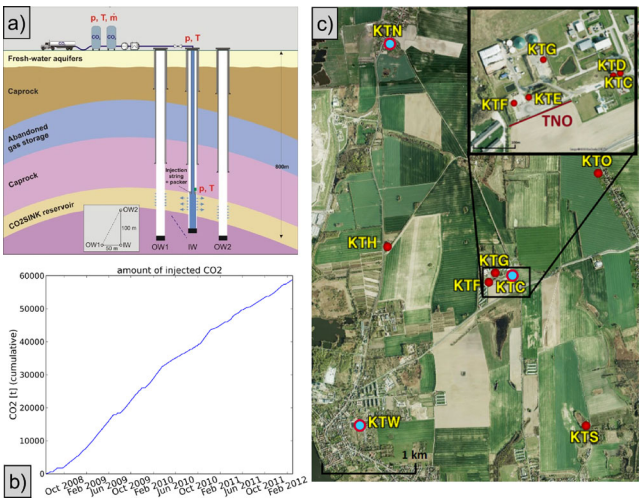

Figure 1. (a) Scheme of CO_2 injection in a saline aquifer at a depth of 650 m, (b) amount of injected CO_2 from 2008 to 2011 and (c) station map of Ketzin, the area around the injection site (close to KTE) is shown in a magnified inset.

in distances of tens of metres up to a few kilometres around the injection site of Ketzin (Fig. 1c). Network operation lasted until 2012 February, when more than 60 000 tons of CO_2 had been injected.

3 AMBIENT NOISE PROPERTIES

We calculated spectrograms at the central station of the array (KTC) to investigate the spectral content of the noise field and its stationarity. Since the direction of incident noise may have changed during the investigated time period within some frequency bands, possibly influencing the measurements of the velocity variations, we also investigated changes of noise directionality at several stations.

3.1 Spectral content of noise

To analyse the spectral content of the noise and its temporal stability, we calculated the spectrogram of the vertical component at station KTC from 2008 June until the end of 2011. In the processing we removed the mean of the data and Fourier transformed time windows of 1 hr length. Since our interest is focused on long term trends, the spectrogram was smoothed with a running mean over periods of 15 d.

The spectrum can be divided into two parts with distinct properties. Below 0.5 Hz it is dominated by the secondary microseismic peak between 0.1 and 0.3 Hz (Fig. 2b). This frequency band is subject to strong annual variations caused by increased wave action in the oceans of the northern hemisphere during northern winter. Significant frequency shifts occur within this band, for example at the end of 2009 January when the storm 'Joris' approached England and moved through Benelux to Germany (IMK & KIT 2013). During this time the peak frequency in the microseismic band shifted from 0.2 to 0.12 Hz (Fig. 2b). Due to the strong annual periodicity, frequency shifts and well-known changes in the directionality of the noise, we exclude this frequency range from the analysis of velocity variations. Instead we focus on frequencies above 0.5 Hz that are excited by local mostly anthropogenic sources. In this band the annual periodicity is much weaker and we do not observe shifts of peak frequencies (Fig. 2a). Temporal variations affect the overall amplitude but not the shape of the spectrum. We therefore expect that the noise sources are excited to a variable degree but their spatial pattern remains stable over time. We will show in the next section that the signal in the 1.0–3.5 Hz band is generated by a wind park. The structure of the spectrogram above 1 Hz with the distinct lines agrees well with the excitation by wind turbines where the 1.4 Hz line corresponds to the blade passing frequency (Saccorotti *et al.* 2011). For monitoring purposes this spectral stability is more important than the higher amplitudes in the microseismic band since frequency shifts can introduce artefacts in measurements of velocity variations (Zhan *et al.* 2013).

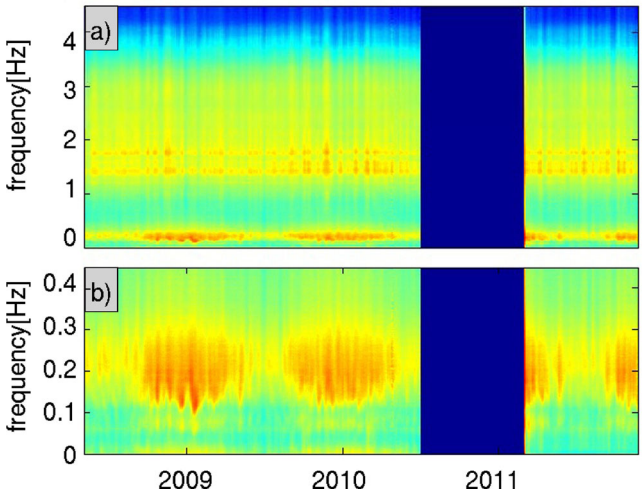

Figure 2. (a) Spectrogram at KTC for 0–5 Hz, (b) same as (a) but for 0–0.45 Hz.

3.2 Direction of noise

Hadziioannou *et al.* (2009) demonstrated that noise based monitoring only requires a stable source distribution in contrast to a complete directional coverage, which is needed for the full convergence towards the Green's function. In the previous section we showed that the spectrum of the noise sources in the 1.0–3.5 Hz band is relatively stable implying a persistent source distribution. To verify this persistence we investigated the directionality of the noise directly.

Our single-station approach estimates the propagation direction of the Rayleigh waves in the ambient noise field using the coherence of horizontal and vertical ground motion. We assume that the noise field consists of an incoherent superposition of body and surface waves. The Rayleigh wave part of the noise field exhibits a 90° phase delay between the vertical component $Z(t)$ and the horizontal component $R(t, \alpha)$ that is rotated into the direction of the incoming noise with an azimuth α. We find the direction of the Rayleigh waves in the noise by maximizing the correlation between the horizontal component and the phase delayed vertical component with respect to the azimuth α:

$$\int_{t_1}^{t_2} \mathcal{H}[Z(t)]R(t,\alpha)\mathrm{d}t \stackrel{!}{=} \max. \tag{1}$$

Here $\mathcal{H}[Z(t)]$ denotes the Hilbert-transform of the vertical component that introduces the 90° phase shift and $R(t, \alpha) = N(t)\cos(\alpha) + E(t)\sin(\alpha)$, where $N(t)$ and $E(t)$ indicate north and east components, respectively. The integral limits t_1 and t_2 denote the time window in the continuous noise record. The first derivative of (1) with respect to α has roots that can be given analytically:

$$\alpha = \arctan \frac{\int_{t_1}^{t_2} \mathcal{H}[Z(t)]E(t))\mathrm{d}t}{\int_{t_1}^{t_2} \mathcal{H}[Z(t)]N(t)\mathrm{d}t}. \tag{2}$$

Since eq. (2) may not only correspond to a maximum in eq. (1) but also to a minimum, the second derivative is considered and a shift of 180° is applied in case it is negative, that is the wave travels in opposite direction.

Before estimating the noise direction α we first tested whether a part of the wavefield exhibits a 90° phase shift between horizontal and vertical displacements to assess the contribution of Rayleigh waves in the noise field. For the test we analysed data of 2 yr from station KTC, selecting short time windows of 20 s length to separate consecutive noise sources as much as possible. We then apply a phase shift φ to the vertical component:

$$Z'(t,\varphi) = \cos(\varphi)Z(t) + \sin(\varphi)\mathcal{H}[Z(t)] \tag{3}$$

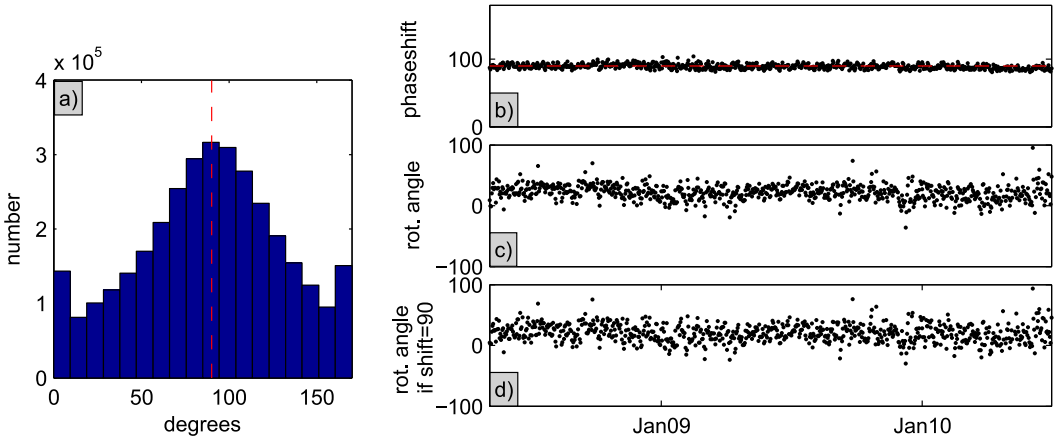

Figure 3. Test for dominance of Rayleigh waves at KTC for a period of 2 yr: (a) histogram of calculated phase shifts φ with maximal coherence between $R(t, \alpha)$ and $Z'(t, \varphi)$, a maximum at 90° shows the dominance of Rayleigh waves, the peaks at 0° and 180° arise from body waves, (b) phase shifts averaged over 1 d, the red line marks a phase shift of 90°, (c) rotation angle α (angle of incoming noise) corresponding to calculated phase shifts, (d) rotation angle if the phase shift is fixed at 90°; (2–2.4 Hz).

and calculate the correlation coefficient between the phase shifted Z' and the R component in a frequency range of 2–2.4 Hz. This process has two free variables: the phase shift φ of the vertical component Z' in the range [0°, 180°) and the azimuth α of R in the range [0°, 360°). Replacing $\mathcal{H}[Z(t)]$ with $Z'(t, \varphi)$ in eq. (1), we estimate for each 20 s time window the pair of α and φ that maximizes eq. (1).

The test calculation for KTC yields a distribution of phase shifts, that is clearly dominated by a peak around 90° indicating that Rayleigh waves dominate the coherence between vertical and horizontal ground motion (Fig. 3a). Body waves causing the peaks at 0 and 180° are also visible. The phase shifts and the corresponding incident angles of noise (Figs 3b and c) are stable in time.

Since the test supports the hypothesis of a dominance of Rayleigh waves, we now use eq. (2) with a fixed phase shift of 90° to investigate the direction of the incident noise field at several stations of the network. As shown in Fig. 3d) fixing the phase shift of the vertical component to 90° does not change the estimated direction of the incident waves. Analysing 2 yr of data at station KTC, KTN and KTW, we find a variation of around 10° with an approximately annual period not exceeding short term fluctuations. We conclude that the distribution of noise field directions is stable and thus allows for robust estimates of velocity changes.

The observed directions of the noise measured at KTC, KTN and KTW point in direction of a wind farm (Fig. 4), whereby the azimuthal fluctuation for KTW, which is furthest away, is narrower than for KTC and KTW, which are closer to the wind farm. In conclusion the seismic noise field in the 1.0–3.5 Hz band at Ketzin is anisotropic but well suited for monitoring as it has a stable spectrum and source distribution.

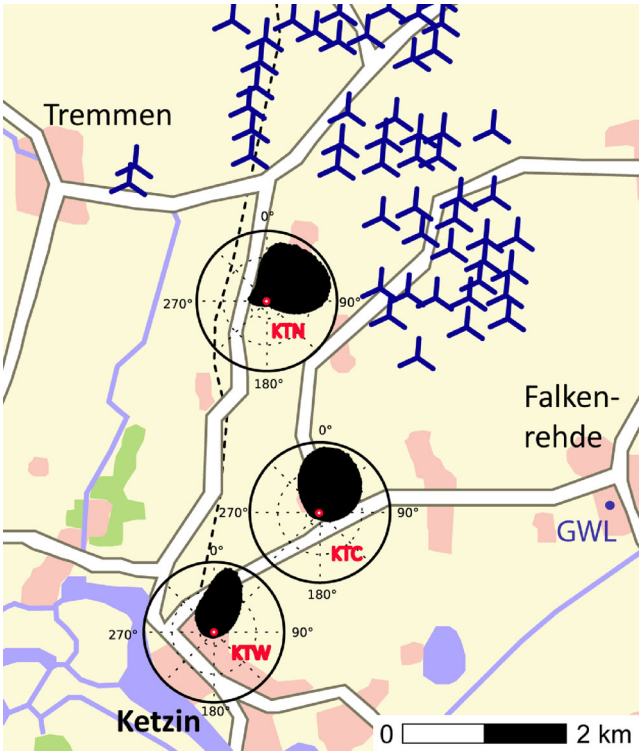

Figure 4. Map of Ketzin, polar-plotted histograms of the calculated angles of incoming noise point towards the wind farm (2–2.4 Hz). GWL indicates the location of the groundwater well.

4 ANALYSIS OF VELOCITY CHANGES

4.1 Selection of the frequency band

The selection of the frequency band for the analysis of temporal variations is crucial for the spatial sensitivity of the measurement which depends on the composition of the wavefield, the traveltime and the subsurface structure. In general the sensitivity of coda waves is a combination of surface wave and body wave sensitivities with gradual transition from surface to body waves with increasing lapse time (Obermann *et al.* 2013). This transition is faster for stronger medium heterogeneity favouring the conversion between the wave types. As surface wave sensitivity is limited to about half the wavelength we aim at a high contribution of body wave sensitivity to enable observations at the reservoir depth. This is favoured by using a high frequency band in which scattering is stronger. Based on this argument and the demonstrated temporal stability of the ambient noise in the 1.0–3.5 Hz for monitoring (Section 3) we focus investigations on this frequency range rather than on the microseismic band.

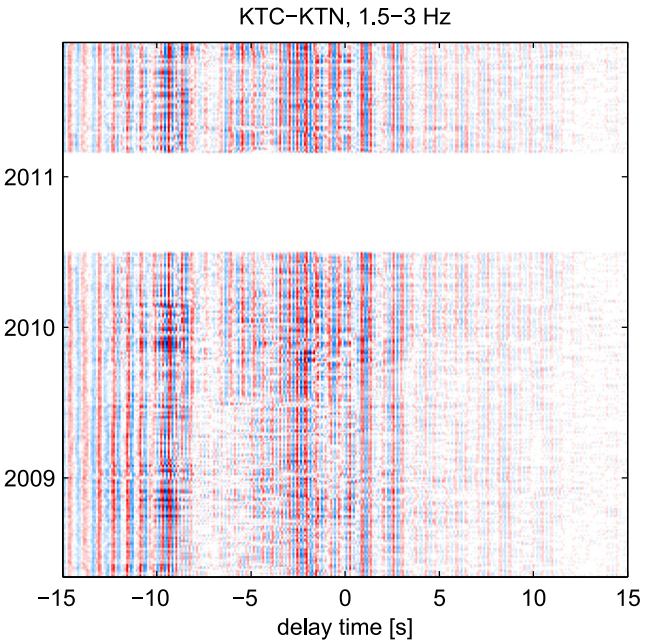

Figure 5. Cross-correlation-matrix KTC-KTN (1.5–3 Hz).

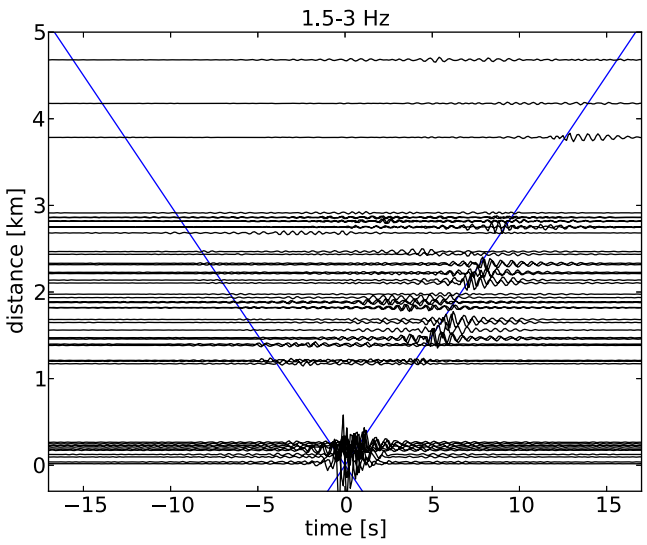

Figure 6. Cross-correlations (1.5–3 Hz), a velocity of 300 m s^{-1} is indicated by blue lines.

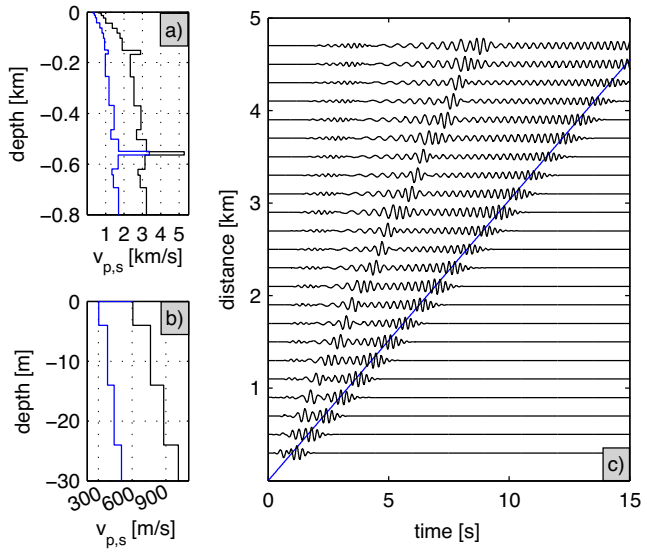

Figure 7. (a) Depth model for v_p (black) and v_s (blue), (b) as (a), but for the upper 30 m, (c) synthetic seismograms (scaled to their maximum) modelled with a free surface (black); a velocity of 303 m s^{-1} is indicated by a blue line.

4.2 Data processing

To retrieve estimates of the Green's functions between the seismic stations, pairwise cross-correlation of 1 hr long segments was applied after rotation of the horizontal components to R- and to T-coordinates (parallel and perpendicular to azimuth between the stations, respectively), followed by the typical time and frequency domain preprocessing: detrending, downsampling to 10 Hz, spectral whitening and 1 Bit normalization (Bensen *et al.* 2007). All 1-hr cross-correlations of 1 d were normalized and stacked to a 1-d cross-correlation.

Occurring clock drifts were corrected following Sens-Schönfelder (2008) because some of the seismometers temporarily had no GPS reception. All cross-correlations show a good coherence over the whole time period (Fig. 5) and are asymmetric as expected from the asymmetry of the noise field. The interruption of the measurements in connection with the re-installation of the stations did not alter the correlation functions.

Arranging all the cross-correlations depending on the interstation distance reveals a dominating phase travelling at about 300 m s^{-1} (Fig. 6). To account for the anisotropy of the noise field the correlation functions are arranged such that energy originating at an azimuth of 20° from the network (direction to the wind park, Section 3.2) causes correlations at positive lag times. This direction best sorts the high and low amplitude sides of the correlation functions confirming the wind park as source region.

4.3 Analysis of the dominating phase in the cross-correlations

One may argue that the velocity of 300 m s^{-1} of the dominating phase, which is close to the speed of sound is produced by air pressure waves coupling to the seismometers. However, we showed in Section 3.2 that the coherence between horizontal and vertical ground motion is in accordance with the propagation of Rayleigh waves and a velocity of 300 m s^{-1} is in agreement with shear wave energy propagating in unconsolidated saturated sediments (Castagna *et al.* 1985; Vernon *et al.* 1998). At the Ketzin site Xu *et al.* (2012) found shear wave velocities of 303.6 m s^{-1} in the shallowest 5 m.

To verify the possibility of energy propagating at 300 m s^{-1} we model the elastic wave propagation in 2-D using the finite differences code sofi2D (Bohlen 2002). As velocity model we use the model of Xu *et al.* (2012) for the top 150 m, combined with the model of Kazemeini *et al.* (2010) for depths down to 700 m as illustrated in Figs 7(a) and (b). Waves are excited by a vertical source with a dominant frequency of 2.25 Hz placed at a depth of 1 m. We used a free surface on top of the model and an absorbing boundary frame with exponential damping at the other three edges. The modelling confirms the possibility of propagation of elastic waves at 303 m s^{-1} in the subsurface structure (Fig. 7c).

4.4 Velocity changes for different station-pairs and components

We analysed possible velocity changes for vertical and for horizontal components, using the stretching method (Sens-Schönfelder & Wegler 2006). A relative velocity change $\mathrm{d}v/v$ leads to a relative time delay of the waveform if the velocity change is spatially homogeneous. Under this assumption the relative time delay is constant and equal to the negative relative velocity change $\epsilon = \mathrm{d}v/v = -\mathrm{d}t/t$, leading to a compression or stretching of the waveform in comparison to the unperturbed state. As the unperturbed signal or so-called reference trace (C_{ref}) we use the mean over all 1-d-cross-correlations of each station pair. For each day we calculated stretched versions of the reference trace for different velocity changes in a range $[\epsilon_1, \ldots, \epsilon_i]$ and computed the correlation coefficient with the 1-d-cross-correlation function $C(t)$:

$$CC(\epsilon_i, t_1, t_2) = \frac{\int_{t_1}^{t_2} C_{\mathrm{ref}}\left(t(1+\epsilon_i)\right) C(t)\mathrm{d}t}{\sqrt{\int_{t_1}^{t_2} C_{\mathrm{ref}}\left(t(1+\epsilon_i)\right)^2 \mathrm{d}t \int_{t_1}^{t_2} C(t)^2 \mathrm{d}t}}. \quad (4)$$

The stretched version with the highest correlation-value with the reference trace then yields the apparent relative velocity change $\mathrm{d}v/v(t_1, t_2) = \underset{\epsilon_i}{\mathrm{argmax}}[CC(\epsilon_i, t_1, t_2)]$.

We analysed moving time windows after the arrival of the 300 m s^{-1} phase using either positive or negative lapse times depending on the signal-to-noise ratio. Figs 8(a)–(c) show the velocity variations for the KTC–KTN station pair in the frequency range of 1.5–3 Hz for ZZ, RR and TT components. Measurements are performed in different time windows of the coda. Values shown in the plot refer to the time after the 300 m s^{-1} phase. For all components we observe velocity variations with a period of approximately one year, which indicates a seasonal environmental influence. In general, the velocity changes estimated from the horizontal components (RR, TT) and the changes estimated from the vertical component (ZZ) are very similar, only the amplitude varies. Errors are calculated following Weaver *et al.* (2011).

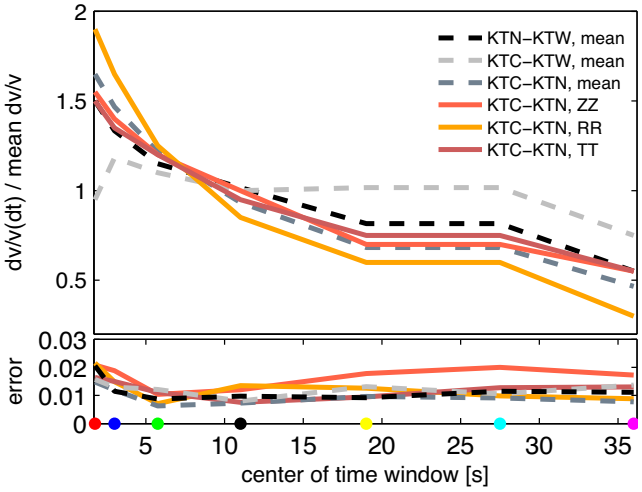

Figure 9. Lapse time dependence of the velocity changes at 1.5–3 Hz as the ratio of velocity change at a particular time window to mean velocity change (mean over all time windows): the ratio is shown for a mean over the vertical and horizontal components of three station-combinations (greyish colours) as well as for every component of the station combination KTC-KTN (reddish colours): the amplitude decay indicates a perturbation in the shallow subsurface (the colour of the dots on the time axis correspond to the colours used for the different time windows in Fig. 8). Errors are shown at the bottom.

To extract information about the lapse time dependence of the apparent velocity changes, we calculated the ratio of velocity changes in the different time windows to the mean velocity change (Fig. 9). Errors were estimated as confidence intervals of the scaling coefficients. In general, amplitudes of the velocity variations systematically decrease for time windows in later parts of the coda. Obermann *et al.* (2013) showed that the depth sensitivity of coda waves can be related to a combination of bulk wave sensitivity and surface wave sensitivity. At early times in the coda, most of the waves propagate as surface waves at shallow depths, and are therefore sensitive to shallow changes. Later in the coda, scattering and mode

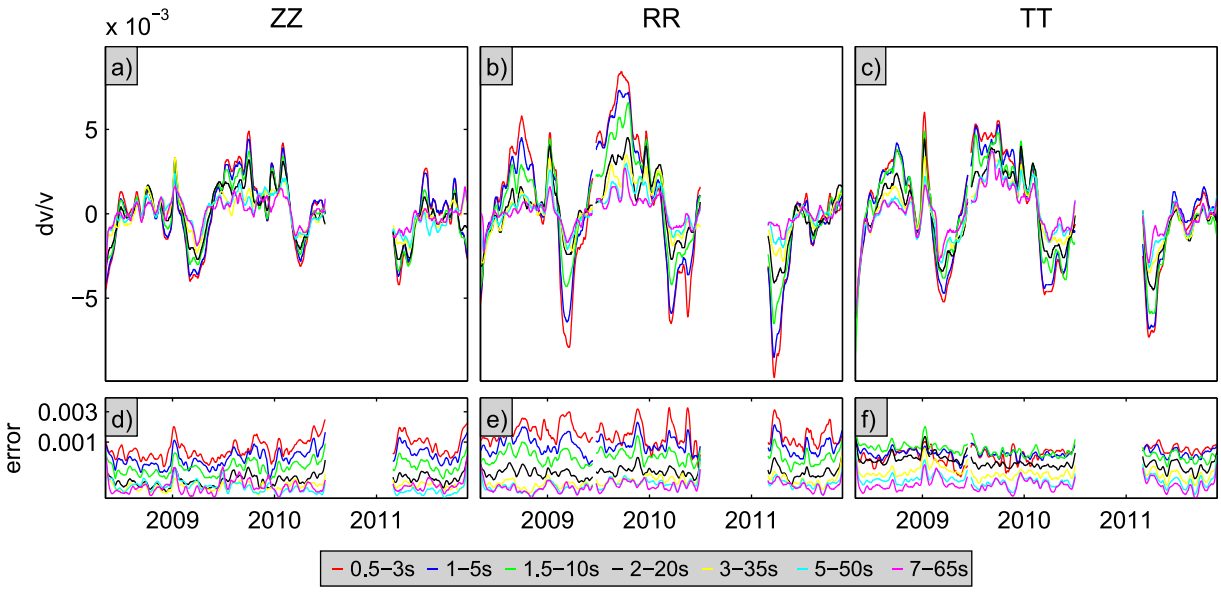

Figure 8. Velocity changes in a frequency range of 1.5–3 Hz for station pair KTC-KTN in different time windows after the 300 m s^{-1} phase as indicated at the bottom: velocity changes for (a) vertical and (b), (c) horizontal components. The corresponding errors are shown in (d), (e) and (f) on a logarithmic scale.

conversion occurred and the waves spent more time in the bulk as body waves, meaning that they are more sensitive to changes at depth. As we observe high amplitudes of the apparent velocity changes at early time windows, the changes must have occurred in the shallow subsurface. This observation is valid for all three station combinations, whereas it is not as significant for KTC-KTW as for the other station-pairs (Fig. 9).

5 DISCUSSION

The periodic velocity variations with an annual cycle dominate our observations. They are visible on all station combinations and on all components. The injection of CO_2 into a porous layer changes the medium and lowers the seismic velocities with respect to a reference state before the injection (Eiken *et al.* 2000; Kazemeini *et al.* 2010; Ivanova *et al.* 2012). Therefore, we expect a monotonic decrease of the seismic velocities over the period of the injection because the injection is almost continuous with a constant rate (on average). However, such a signal cannot be observed.

The analysed frequency range of 1.5–3 Hz may be too high for observing possible velocity changes due to the CO_2-storage at a depth of 650 m with surface waves. The depth sensitivity kernels for phase velocity of Rayleigh waves to perturbations in shear velocity, based on the depth model in Fig. 7 show that the highest sensitivity at the depth of the storage site is around 0.7 Hz. The sensitivity of waves in this frequency range to changes at the shallow subsurface is not negligible, meaning that the influence of the shallow subsurface cannot be avoided. Furthermore, 0.7 Hz is in the middle of a relatively quiet frequency band, as shown in Fig. 2. However, we also estimated velocity changes around 0.7 Hz, but short termfluctuations exceeded every kind of long term trend. We therefore selected the high frequency band between 1.5 and 3 Hz because we expect that scattering is stronger and the body wave contribution is higher than for lower frequencies (Section 3.1).

The fact, that the observed velocity changes in Ketzin are shallow and show an annual periodicity indicates that environmental effects like temperature, precipitation or a change in the groundwater level (GWL) play a significant role in the generation of the velocity changes. Due to the moderate climate we expect that hydrological changes dominate over the effects of temperature induced thermoelastic strain (Ben-Zion & Leary 1986). We therefore compare our estimates with different hydrological measurements.

5.1 Comparison of annual velocity changes with modelled soil moisture

Moisture could be a candidate for seasonal variations: as the weathered zone gets moist or dry depending on meteorological and seasonal conditions, seismic wave velocity varies instantly because the geomechanical properties of this layer are altered by water presence. Therefore, if moisture is driving the velocity changes at the Ketzin site, we should see a correlation without time shift between moisture and velocity changes. To analyse the relation of moisture on the periodic velocity changes we use modeled soil moisture data for depths down to 60 cm (provided by Deutscher Wetterdienst, Abteilung Agrarmeteorologie). The model takes into account meteorological data from a weather station in Potsdam at a distance of approximately 17 km from Ketzin, as well as the type of soil and vegetation. We compared the velocity variations with soil moisture modelled for grass coverage and without vegetation cover because it best represents the local conditions at the stations and the surrounding farmland. In general, both models show a maximum of soil moisture in winter and a minimum in summer, whereas the velocity changes show a maximum in November and a minimum at the end of March. This phase delay between the observed velocity variations and the modelled soil moisture excludes the soil moisture as cause of the velocity variations.

5.2 Comparison of annual velocity changes with GWL

The Ministry of Environment, Health and Consumer Protection of the Federal State of Brandenburg operates a monitoring program to ascertain the groundwater properties and level. We use GWL data from a monitoring well in Falkenrehde, which is approximately 3.7 km east of the injection site (Fig. 4). The material at the depth of the GWL (approximately 5.5 m below surface) consists of a weak gravelly fine sand. A direct correlation between GWL and velocity variations is expected because the sensitivity of the velocity measurements is almost constant over the small depth range of about 50 cm affected by the GWL variations.

We find a remarkable correlation between the velocity changes and the GWL (Fig. 10a). A rise in the GWL introduces a decrease in the seismic velocities.

According to the theory of Gassmann (1951), which describes the fluid-saturation effects in porous rocks, a change in saturation affects both density and effective bulk modulus. In the linear regime with a water saturation below a critical value, the *P*-wave velocity decreases with increasing saturation due to the replacement of air with water in pore spaces, leading to a higher density. When the saturation exceeds the critical value the effective bulk modulus and the *P*-wave velocity show a rapid and nonlinear increase due to the fluid compressibility. Theory predicts 99 per cent for the critical saturation value, but in practice the critical saturation can be 80 per cent (Gaines *et al.* 2010). This means that if the *P*-wave velocity follows the trend in our data the dominant effect is not a velocity increase below the GWL. Rather the increased saturation in the

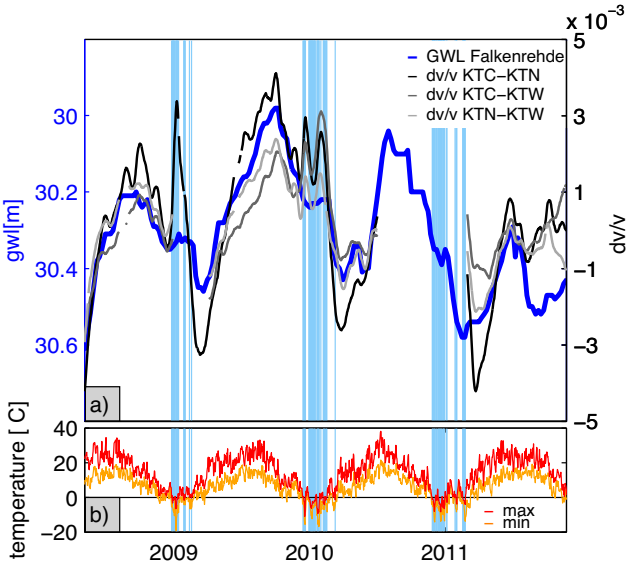

Figure 10. Comparison of velocity change to groundwater level (GWL). (a) Mean velocity variations (grey) compared with GWL in Falkenrehde (blue), (GWL is in m above sea level, note the reversed axis orientation), (b) minimum and maximum (orange/red) temperature per day, times where the maximum temperature is below 0 °C are highlighted in light blue.

soil above the GWL that accompanies the accelerated infiltration in periods of high GWL leads to a decrease in *P*-wave velocity. This concept is supported by the observation of consistently delayed arrival times in the second of two time lapse campaigns in our study area (Kashubin *et al.* 2011). The second campaign took place at a time with higher precipitation and increased GWL.

The second concept to be considered when interpreting the relation between our measurements and the GWL is that the sensitivity of scattered bulk waves and surface waves to *S*-wave velocity is much higher than to *P*-wave velocity. This directly follows from considerations of equipartition in the scattered coda wavefield (Weaver 1990; Ryzhik *et al.* 1996), that predicts a ratio of energy densities for long propagation times of $E_s/E_p = 2v_p^3/v_s^3 \approx 10.4$ under the assumption $v_p/v_s = \sqrt{3}$. Experimental results measured with a small-aperture seismic array in Mexico show that the ratio can be a bit lower (Shapiro *et al.* 2000). The small sensitivity of the shear modulus to changes in water saturation can lead to an opposite behaviour of saturation and velocity due to the density changes. Such an effect is supported by observations of West & Menke (2000) who repeatedly carried out an active seismic experiment at a beach during a tidal cycle and observed a decrease in shear velocity from low tide to high tide. Similar to our observations Sens-Schönfelder & Wegler (2006) found a clear relation between a precipitation derived model for GWL at Merapi volcano and velocity variations.

The difference between the GWL changes and the velocity changes is of the same order as the variances of the velocity changes measured for different station pairs. We thus attribute this mismatch to lateral variations in the subsurface.

5.3 Influence of ground frost

Apart from the good agreement between the GWL and velocity data there are distinct episodes of mismatch between these curves during winter time. Fig. 10(b) shows the minimum and maximum temperature per day in Potsdam. If the maximal daily temperature decreases below 0 °C, the upper part of ground freezes. During these days the velocity curves vary significantly from the curve of the GWL: While the GWL stays nearly constant, the velocity suddenly increases at the onset of such a period (Fig. 10). When temperatures increase again and the soil thaws we observe a drastic decrease of velocity that overshoots the prior increase.

We interpret this as the consequence of the strong increase of the shear modulus in comparison to the unfrozen soil. The strong decrease after the frost periods most probably results from the melting of snow and the fast infiltration of water in the subsurface as documented by the increase of the GWL after frost periods.

6 CONCLUSIONS AND OUTLOOK

The application of PII to seismic data recorded at the CO_2 storage test site in Ketzin reveals clear periodic variations of subsurface velocities measured consistently at different station pairs and different components. The variations are not caused by changes in the characteristics of the noise field as its spectral content and distribution of propagation directions are stable. The analysis in different lag-time windows showed that the velocity perturbations must originate in the shallow subsurface. This is confirmed by the annual periodicity of the velocity changes that correlates with changes in the GWL. The strongest deviations between groundwater level and velocity changes are observed during winter when the maximum temperature lies below the freezing point. This indicated that strong short term fluctuations in the velocity changes in winter time are caused by ground frost. Potential signals related to the spreading of the CO_2 plume in the reservoir at 650 m depth are hidden in the signals caused by groundwater changes and frost.

With the current approach it was not possible to monitor velocity changes related to the CO_2 storage with the coda of ambient noise correlations from seismic surface records but there are strategies to increase the sensitivity at the reservoir depth and to reduce the influence of the near-surface changes. A first strategy would be the use of borehole sensors. The noise correlation function only approximates the Green's function and is overprinted by the characteristics of the noise field. Thus, a deeper sensor will first reduce the dominance of surface wave modes with large amplitudes and high sensitivity in shallow layers. Secondly, a downhole observation will also shift the partitioning between surface and body waves towards the latter because the bulk wave amplitudes do not decay with depth. A second possibility is to actively select time periods with increased body wave portion in the 'noise' signal to enforce the retrieval of body waves in the cross-correlations. Especially useful in this context are records of seismic coda waves of earthquakes. These signals represent a mixture of scattered surface and body waves that is excited by a source in the bulk and thus has a stronger body wave component. For the retrieval of teleseismic body waves Zhan *et al.* (2010) and Lin *et al.* (2013) demonstrated the importance of the coda wavefield of large earthquakes. There might be the possibility to take advantage of this concept in a local small scale application. Another part of a strategy to increase the sensitivity at the reservoir could be the application of beamforming techniques during the noise correlation. With a seismic array it is possible to form a beam with specific directional characteristics to perform a double beamforming in the correlation that can significantly increase the retrieval of body waves and enhance the sensitivity at specific target areas (Boue *et al.* 2013). The application of these strategies is beyond the analysis in this study but with the installation of a downhole array by TNO (Netherlands Organization for Applied Scientific Research) (Fig. 1, Arts *et al.* 2011) the injection site offers all requirements and this data should be analysed in detail before judging about the general capabilities of seismic interferometry for monitoring CO_2 migration in the subsurface.

ACKNOWLEDGEMENTS

We acknowledge support from the BMBF GeoTechnologien Program Tomographie under the grant MIIC FKZ: 03G0736A and we are grateful for support by the Ketzin Pilot Site research group. We also thank the Ministry of Environment, Health and Consumer Protection of the Federal State of Brandenburg for providing the groundwater data. In 2011 we used seismometers provided by the Geophysical Instrument Pool Potsdam (GIPP) of the GFZ.

REFERENCES

Arts, R., Eiken, O., Chadwick, A., Zweigel, P., van der Meer, B. & Kirby, G., 2004. Seismic monitoring at the Sleipner underground CO_2 storage site (North Sea), *Geol. Soc., Lond., Spec. Publ.,* **233**(1), 181–191.

Arts, R. *et al.*, 2011. Results of a monitoring pilot with a permanent buried multicomponent seismic array at Ketzin, *Energy Procedia,* **4,** 3588–3595.

Ben-Zion, Y. & Leary, P., 1986. Thermoelastic strain in a half-space covered by unconsolidated material, *Bull. seism. Soc. Am.,* **76**(5), 1447–1460.

Bensen, G.D., Ritzwoller, M.H., Barmin, M.P., Levshin, A.L., Lin, F., Moschetti, M.P., Shapiro, N.M. & Yang, Y., 2007. Processing seismic

ambient noise data to obtain reliable broad-band surface wave dispersion measurements, *Geophys. J. Int.,* **169**(3), 1239–1260.

Bohlen, T., 2002. Parallel 3-D viscoelastic finite difference seismic modelling, **28,** 887–899.

Boue, P., Poli, P., Campillo, M., Pedersen, H., Briand, X. & Roux, P., 2013. Teleseismic correlations of ambient seismic noise for deep global imaging of the Earth, *Geophys. J. Int.,* **194**(2), 844–848.

Brenguier, F., Shapiro, N.M., Campillo, M., Nercessian, A. & Ferrazzini, V., 2007. 3-D surface wave tomography of the Piton de la Fournaise volcano using seismic noise correlations, *Geophys. Res. Lett.,* **34**(2), 1–5.

Brenguier, F., Campillo, M., Hadziioannou, C., Shapiro, N.M., Nadeau, R.M. & Larose, E., 2008a. Postseismic relaxation along the San Andreas fault at Parkfield from continuous seismological observations, *Science (New York, N.Y.),* **321**(5895), 1478–1481.

Brenguier, F., Shapiro, N.M., Campillo, M., Ferrazzini, V., Duputel, Z., Coutant, O. & Nercessian, A., 2008b. Towards forecasting volcanic eruptions using seismic noise, *Nat. Geosci.,* **1**(2), 126–130.

Campillo, M., 2006. Phase and correlation in 'random' seismic fields and the reconstruction of the Green function, *Pure appl. Geophys.,* **163**(2–3), 475–502.

Campillo, M. & Paul, A., 2003. Long-range correlations in the diffuse seismic coda, *Science,* **299,** 547–549.

Castagna, J., Batzle, M. & Eastwood, R., 1985. Relationships between compressional-wave and shear-wave velocities in clastic silicate rocks, *Geophysics,* **50**(4), 571–581.

Eiken, O., Brevik, I., Arts, R., Lindeberg, E. & Fagervik, K., 2000. Seismic monitoring of CO_2 injected into a marine aquifer, in *Proceedings of the SEG Calgary 2000 International Conference and 70th Annual Meeting,* Calgary, paper RC-8.2.

Förster, A. *et al.*, 2006. Baseline characterization of the CO2SINK geological storage site at Ketzin, Germany, *Environ. Geosci.,* **13**(3), 145–161.

Gaines, D., Baker, G.S., Hubbard, S.S., Watson, D., Brooks, S. & Jardine, P., 2010. Detecting perched water bodies using surface-seismic time-lapse traveltime tomography, in *Advances in Near-Surface Seismology and Ground-Penetrating Radar: Geophysical Developments Series 15,* Chap. 25, pp. 415–428, eds Miller, R.D., Bradford, J.H. & Holliger, K., SEG.

Gassmann, F., 1951. Über die Elastizität poröser Medien, *Vierteljahrsschrift der Naturforschenden Gesselschaft in Zürich,* **96,** 1–23.

Hadziioannou, C., Larose, E. & Coutant, O., 2009. Stability of monitoring weak changes in multiply scattering media with ambient noise correlation: laboratory experiments, *J. acoust. Soc. Am.,* **125,** 3688.

Hillers, G., Campillo, M. & Ma, K.-F., 2014. Seismic velocity variations at TCDP are controlled by MJO driven precipitation pattern and high fluid discharge properties, **391,** 121–127.

Hobiger, M., Wegler, U., Shiomi, K. & Nakahara, H., 2012. Coseismic and postseismic elastic wave velocity variations caused by the 2008 Iwate-Miyagi Nairiku earthquake, Japan, *J. geophys. Res.,* **117**(B9), 1–19.

IMK KIT 2013. Available at: http://www.wettergefahren-fruehwarnung.de/Ereignis/20090128_e.html, last accessed 27 November 2013.

Ivanova, A., Kashubin, A., Juhojuntti, N., Kummerow, J., Henninges, J., Juhlin, C., Lüth, S. & Ivandic, M., 2012. Monitoring and volumetric estimation of injected CO_2 using 4D seismic, petrophysical data, core measurements and well logging: a case study at Ketzin, Germany, *Geophys. Prospect.,* **60**(5), 957–973.

Juhlin, C. *et al.*, 2007. 3D baseline seismics at Ketzin , Germany: the CO_2 SINK project, *Geophysics,* **72**(5), B121–B132.

Kashubin, A., Juhlin, C., Malehmir, A., Lüth, S., Ivanova, A. & Juhojuntti, N., 2011. A footprint of rainfall on land seismic data repeatability at the CO_2 storage pilot site, Ketzin, in *Proceedings of the SEG San Antonio 2011 Annual Meeting,* 18–23 September, San Antonio, TX, pp. 4165–4169.

Kazemeini, S.H., Juhlin, C. & Fomel, S., 2010. Monitoring CO_2 response on surface seismic data: a rock physics and seismic modeling feasibility study at the CO_2 sequestration site, Ketzin, Germany, *J. appl. Geophys.,* **71**(4), 109–124.

Larose, E. *et al.*, 2006. Correlation of random wavefields: an interdisciplinary review, *Geophysics,* **71**(4), SI11–SI21.

Lin, F.-C., Ritzwoller, M.H. & Snieder, R., 2009. Eikonal tomography: surface wave tomography by phase front tracking across a regional broad-band seismic array, *Geophys. J. Int.,* **177,** 1091–1110.

Lin, F.-C., Tsai, V.C., Schmandt, B., Duputel, Z. & Zhan, Z., 2013. Extracting seismic core phases with array interferometry, *Geophys. Res. Lett.,* **40**(6), 1049–1053.

Mainsant, G., Larose, E., Brönnimann, C., Jongmans, D., Michoud, C. & Jaboyedoff, M., 2012. Ambient seismic noise monitoring of a clay landslide: toward failure prediction, *J. geophys. Res.,* **117**(F1), F01030, doi:10.1029/2011JF002159.

Meier, U., Shapiro, N.M. & Brenguier, F., 2010. Detecting seasonal variations in seismic velocities within Los Angeles basin from correlations of ambient seismic noise, *Geophys. J. Int.,* **181**(2), 985–996.

Nishida, K., 2013. Global propagation of body waves revealed by cross-correlation analysis of seismic hum, *Geophys. Res. Lett.,* **40**(9), 1691–1696.

Obermann, a., Planes, T., Larose, E., Sens-Schönfelder, C. & Campillo, M., 2013. Depth sensitivity of seismic coda waves to velocity perturbations in an elastic heterogeneous medium, *Geophys. J. Int.,* **194**(1), 372–382.

Poli, P., Pedersen, H.A., Campillo, M. & the POLENET/LAPNET Working Group, 2012. Emergence of body waves from cross-correlation of short period seismic noise, *Geophys. J. Int.,* **188**(2), 549–558.

Poupinet, G., Ellsworth, W. & Frechet, J., 1984. Monitoring velocity variations in the crust using earthquake doublets: an application to the Calaveras Fault, California, *J. geophys. Res.,* **89**(4), 5719–5731.

Riahi, N., Bokelmann, G., Sala, P. & Saenger, E.H., 2013. Time-lapse analysis of ambient surface wave anisotropy: a three-component array study above an underground gas storage, *J. geophys. Res.: Solid Earth,* **118**(10), 5339–5351.

Richter, T., Sens-Schönfelder, C., Kind, R. & Asch, G., 2014. Comprehensive observation and modeling of earthquake and temperature-related seismic velocity changes in Northern Chile with passive image interferometry, *J. geophys. Res.: Solid Earth,* **119**(6), 4747–4765.

Ringrose, P., Atbi, M., Mason, D., Espinassous, M., Myhrer, O.y., Iding, M., Mathieson, A. & Wright, I., 2009. Plume development around well KB-502 at the In Salah CO_2 storage site, *First Break,* **27,** 85–89.

Roux, P., 2005. P-waves from cross-correlation of seismic noise, *Geophys. Res. Lett.,* **32**(19), L19303, doi:10.1029/2005GL023803.

Ryzhik, L.V., Papanicolaou, G.C. & Keller, J.B., 1996. Stability of the P to S ratio in the diffusive regime, *Wave Motion,* **24,** 327–370.

Saccorotti, G., Piccinini, D., Cauchie, L. & Fiori, I., 2011. Seismic noise by wind farms: a case study from the Virgo Gravitational Wave Observatory, Italy, *Bull. seism. Soc. Am.,* **101**(2), 568–578.

Sens-Schönfelder, C., 2008. Synchronizing seismic networks with ambient noise, *Geophys. J. Int.,* **174**(3), 966–970.

Sens-Schönfelder, C. & Larose, E., 2010. Lunar noise correlation, imaging and monitoring, *Earthq. Sci.,* **23**(5), 519–530.

Sens-Schönfelder, C. & Wegler, U., 2006. Passive image interferometry and seasonal variations of seismic velocities at Merapi Volcano, Indonesia, *Geophys. Res. Lett.,* **33**(21), 1–5.

Sens-Schönfelder, C. & Wegler, U., 2011. Passive image interferometry for monitoring crustal changes with ambient seismic noise, *Comp. Rend. Geosci.,* **343**(89), 639–651.

Sens-Schönfelder, C., Pomponi, E. & Peltier, A., 2014. Dynamics of Piton de la Fournaise volcano observed by passive image interferometry with multiple references, *J. Volc. Geotherm. Res.,* **276**(0), 32–45.

Shapiro, N.M., Campillo, M., Margerin, L., Singh, S.K., Kostoglodov, V. & Pacheco, J., 2000. The energy partitioning and the diffusive character of the seismic coda, *Bull. seism. Soc. Am.,* **3**(90), 655–665.

Shapiro, N.M., Campillo, M., Stehly, L. & Ritzwoller, M.H., 2005. High-resolution surface-wave tomography from ambient seismic noise, *Science,* **307,** 1615–1618.

Snieder, R., 2004. Extracting the Green's function from the correlation of coda waves: a derivation based on stationary phase, *Phys. Rev. E,* **96,** 046610-1–046610-8.

Snieder, R., Grêt, A., Douma, H. & Scales, J., 2002. Coda wave interferometry for estimating nonlinear behaviour in seismic velocity, *Science,* **295**(3), 2253–2255.

Stehly, L., Campillo, M., Shapiro, N.M., Fry, B. & Boschi, L., 2009. Tomography of the Alpine region from observations of seismic ambient noise, *J. geophys. Res.,* **178,** 338–350.

Tonegawa, T., Nishida, K., Watanabe, T. & Shiomi, K., 2009. Seismic interferometry of teleseismic S-wave coda for retrieval of body waves: an application to the Philippine Sea slab, *Geophys. J. Int.,* **178,** 1574–1586.

Tsai, V.C., 2011. Understanding the amplitudes of noise correlation measurements, *J. geophys. Res.,* **116**(B9), 1–16.

Vernon, F.L., Pavlis, G.L., Owens, T.J., McNamara, D.E. & Anderson, P.N., 1998. Near-surface scattering effects observed with a high-frequency phased array at Pineon flats, California, *Bull. seism. Soc. Am.,* **88**(6), 1548–1560.

Wapenaar, K., 2004. Retrieving the elastodynamic Green's function of an arbitrary inhomogeneous medium by cross correlation, *Phys. Rev. Lett.,* **93,** doi:10.1103/PhysRevLett.93.254301.

Weaver, R., 1990. Diffusivity of ultrasound in polycrysta, *J. Mech. Phys. Solids,* **38**(1), 55–86.

Weaver, R.L. & Lobkis, O.I., 2004. Diffuse fields in open systems and the emergence of the Green's function (L), *J. acoust. Soc. Am.,* **116**(5), 2731–2734.

Weaver, R.L., Hadziioannou, C., Larose, E. & Campillo, M., 2011. On the precision of noise correlation interferometry, *Geophys. J. Int.,* **185**(3), 1384–1392.

Wegler, U., Nakahara, H., Sens-Schönfelder, C., Korn, M. & Shiomi, K., 2009. Sudden drop of seismic velocity after the 2004 Mw 6.6 mid-Niigata earthquake, Japan, observed with passive image interferometry, *J. geophys. Res.,* **114**(B6), 1–11.

West, M. & Menke, W., 2000. Fluid-induced changes in shear velocity from surface waves, in *Proceedings of the Symposium on the Application of Geophysics to Engineering and Environmental Problems (SAGEEP),* Chap. 2, pp. 21–28, SEG.

Xu, Z., Juhlin, C., Gudmundsson, O., Zhang, F., Yang, C., Kashubin, A. & Lüth, S., 2012. Reconstruction of subsurface structure from ambient seismic noise: an example from Ketzin, Germany, *Geophys. J. Int.,* **189,** 1085–1102.

Zhan, Z., Ni, S., Helmberger, D.V. & Clayton, R.W., 2010. Retrieval of Moho-reflected shear wave arrivals from ambient seismic noise, *Geophys. J. Int.,* **182**(1), 408–420.

Zhan, Z., Tsai, V.C. & Clayton, R.W., 2013. Spurious velocity changes caused by temporal variations in ambient noise frequency content, *Geophys. J. Int.,* **194**(3), 1574–1581.